Open source toolkit for temporally controlled rodent behavior suitable for electrophysiology and optogenetic manipulations

Nicola Solari[1,*], Katalin Sviatkó[1,2,*], Tamás Laszlovszky[1,2,*], Panna Hegedüs[1,*], Balázs Hangya[1]

[1] Lendület Laboratory of Systems Neuroscience, Department of Cellular and Network Neurobiology, Institute of Experimental Medicine, Hungarian Academy of Sciences, Budapest, Hungary

[2] János Szentágothai Doctoral School of Neurosciences, Semmelweis University, Budapest, Hungary

*, These authors contributed equally to this work.

Correspondance:

Balázs Hangya
hangya.balazs@koki.mta.hu

Keywords: sensory stimulus, reinforcement, measurement noise, sound attenuation, temporal control, head-fixed

Abstract

Understanding how the brain controls behavior requires observing and manipulating neural activity in awake behaving animals. Neuronal firing is timed at millisecond precision. Therefore, to decipher temporal coding, it is necessary to monitor and control animal behavior at the same level of temporal accuracy. However, commonly available processors are not designed for this task and it is challenging to deliver sensory stimuli and reinforcers as well as to read the behavioral responses they elicit with millisecond precision. We present here a set of tools that offer affordable solutions to achieve these goals, including a physical environment to train head-fixed animals, means of providing calibrated sound stimuli and technical details of delivering sensory cues, fluid reward and air puff punishment with measured latencies. Combined with electrophysiology and optogenetic manipulations, the millisecond timing accuracy will help interpret temporally precise neural signals and behavioral changes. Additionally, since software and hardware provided here can be readily customized to achieve a large variety of paradigms, these solutions enable an unusually flexible design of rodent behavioral experiments.

Introduction

Mechanistic insight about brain function often comes from accurate recordings of action potentials fired by neurons at millisecond order temporal precision. For instance, to understand how specific information about external stimuli and internal variables is encoded in neural firing patterns, researchers have to measure action potentials from awake, behaving animals (Kayser et al., 2010; Panzeri et al., 2017; Tiesinga et al., 2008; Zuo et al., 2015). Moreover, to have sufficient statistical power to resolve key features of the neural code, animals have to repeat these tasks multiple times in a single recording session (Panzeri et al., 2017). Thus the workflow in behavioral neurophysiology labs typically has two stages: 1. train animals on a behavioral task of interest and 2. record their neuronal activity while they perform the task.

The high temporal precision of neuronal firing has strong implications for the scope of suitable behavioral tasks. Intuitively, one can only hope to extract specific information about external variables carried by spike timing (Arabzadeh et al., 2006; Panzeri et al., 2017) if behaviorally relevant events of the task, like cue stimuli (Brunton et al., 2013; Hanks et al., 2015; Jaramillo and Zador, 2011; Ranade and Mainen, 2009; Raposo et al., 2012), go and stop instructions (Lin and Nicolelis, 2008), reward and punishment delivery (Cohen et al., 2012; Hangya et al., 2015; Pi et al., 2013) are under the same precision of temporal control. This intuition is formally captured by Shannon's framework of information channel capacity, also known as the 'Shannon limit', which quantifies the maximal rate of error-free information transfer through a channel with given bandwidth and noise (Csiszár and Körner, 2011).

The first step of analyzing awake recordings is often the calculation of event-aligned spike rasters and different forms of peri-event firing averages (Endres et al., 2008; Shimazaki and Shinomoto, 2010). In these, neural activity is averaged across multiple trials aligned to reoccurring events to provide a statistically robust mean firing activity correlated with the event of interest (Figure 1). This can then be used for instance to interpret the impact of external stimulation on firing rate (Lima et al., 2009) (peri-stimulus time histogram; Figure 1A), to find behavior correlates of specific cell types (Cohen et al., 2012; Hangya et al., 2015; Kvitsiani et al., 2013) (Figure 1B) or to quantify the information about sensory events conveyed by neural activity (Arabzadeh et al.,

2006; Diamond et al., 2008; Zuo et al., 2015) (Figure 1C). However, this approach is limited by the available timing information of the aligning event: any unobserved variation of event timing adds to the spiking noise and is mathematically inseparable from biological variation in neural activity (Figure 2). Therefore it is paramount to control and observe the aligning events to the maximal possible accuracy, at least matching the temporal precision of spike timing, necessitating millisecond order precision.

However, standard operating systems and software are not suitable for this task (but see http://rtxi.org/). Indeed, the time from command to task execution varies between times orders of magnitudes longer than desired and is influenced by background processes like scheduled system maintenance or security scans. Real-time operation systems can be used to achieve submillisecond behavior control (Brunton et al., 2013; Jaramillo and Zador, 2011; Poddar et al., 2013). However, the emergence of affordable microcontrollers that are easy to program provide a unique opportunity to build modular, flexible and cheap behavior control systems suitable for millisecond order precision.

We present and validate a behavioral setup, leveraging an open source behavior system to achieve millisecond precision hardware control, and demonstrate that our setup is suitable for combined neural recordings and optogenetic stimulation. First, we describe a custom fabricated sound attenuated behavioral chamber and provide a configuration for combined behavior, electrophysiology and optogenetics experiments in head-fixed mice. Second, we describe temporally precise delivery of calibrated audiovisual sensory cues and reinforcers.

Methods

Sound Calibration

Pure tones were generated in Matlab as sine waves. The tones were uploaded as .wav files to a USB-based microcontroller development system Teensy 3.2 and its audio adaptor board (TEENSY32 and TEENSY3_AUDIO, PJRC) using the Bpod r0.5 behavior control system (Sanworks LLC, www.sanworks.io). The uploaded tracks were played applying Bpod commands controlled by custom-written MATLAB code (https://github.com/hangyabalazs/Rodent_behavior_setup/tree/master/sound_calibration). The Teensy adaptor board's jack output was connected to an Adafruit audio amplifier Stereo 20w Class D (MAX9744, Adafruit) attached to 8 Ohm Magnetic Speakers (668-1447-ND, Digikey) positioned on the left and right side of the behavioral chamber. A calibrated precision electret condenser microphone (EMM-6, Daytonaudio) was connected to a preamplifier digital converter (AudioBox iOne, PreSonus) and placed in the behavioral enclosure to model the position of the animal's head in a head-fixed configuration. The dB-SPL levels registered by the microphone were read using the free version of TrueRTA software, a commercial audio analysis software package (TrueRTA, True Audio) and fed back to the custom developed calibration software (Figure 6A-B).

Measuring the delay of visual cues

All delays were measured by sending command signals from Bpod on two different outputs: the BNC output port and the RJ45 connector for communication with the PCB board connecting Bpod to a behavior port ('port interface board', https://sanworks.io/shop/viewproduct?productID=1008). First, we measured the 'internal' delay

in addressing these two ports, i.e. the average minimal temporal difference between sending signals on these connectors by Bpod (Figure 3A). The time difference between the two signals was of 0.045 ± 0.001 ms (mean ± SD, n=180 repeats; see Figure 7A for distribution). This 50 microsecond delay adds only negligible noise to our delay measurements that are on the millisecond order; therefore, we refer to the two signals as 'concurrent' hereinafter.

To determine the temporal delay between the command signal and the voltage signal sent directly to the LED, a PC oscilloscope (PicoScope 2204A, Pico Technology) was connected to the LED output wire terminal of the port interface board (Figure 3B). Concurrent with the command signal to the board, a TTL pulse was sent to the oscilloscope from the Bpod BNC output terminal. We determined the distribution of temporal differences between the above two signals using oscilloscope measurements (n = 180 repeats).

Measuring the delay of sound delivery

Sounds were delivered using an audio adaptor board (Audio Adaptor Board for Teensy 3, PJRC) and a microcontroller development system (Teensy USB Development Board 3.2, PJRC) connected to Bpod. To measure the time delay between the command signal and the digital sound signal, the PC oscilloscope was connected to the line out pins of the Audio Adaptor Board (Figure 3C). Whenever a tone was triggered, the signal was detected by the oscilloscope. A BNC cable connected the Bpod module BNC output channel directly to the oscilloscope: the commands for triggering a sound and for sending a TTL pulse were elicited simultaneously and the time difference between the board output and the Bpod TTL was measured as the sound delivery delay. We determined the distribution of temporal differences between the above two signals using oscilloscope measurements (n = 180 repeats).

Measuring the delay of reinforcement delivery

Air and water delivery was controlled by a 12V solenoid valve (LHDA0531115H, The Lee Company) connected to the Bpod port interface board. The air and water reservoirs were connected to the valves by Nalgene 180 Clear Plastic PVC Metric Tubing (ID, 2 mm; OD, 4 mm; Thermo Scientific 8001-0204); the same tubing was used between the valves and the lick port. The lick port was equipped by small pieces of polyethylene tubing (ID, 1.14 mm; OD, 1.57 mm; Warner Instruments 64-0755/PE-160) on the output side. The PC oscilloscope was connected to the LED output wire terminal of the port interface board, but the circuit was kept open leaving a small gap (less than 1mm) between the wire from the port interface board and the one connected to the oscilloscope input. The end of the water delivery tubing was placed directly to the gap. Power output was constantly provided to the LED terminal, so upon water outflow the circuit closed and a voltage change could be detected (Figure 3D). To measure the water delivery delay, a TTL pulse was sent to the oscilloscope from the Bpod BNC output terminal in parallel with the logic pulse to the port interface board. The delay was the difference between the signal caused by closing the circuit via the LED terminal and the TTL sent from the Bpod BNC output. The delay of air puff delivery was measured similarly but the circuit through the LED terminal of the port interface board was closed by a small drop of water before measurement and the outflow of air disconnected this circuit. Delay was measured as the time difference between the drop of the signal through the port interface board and the rising edge of the TTL from the Bpod BNC output (n = 60 repeats for each reinforcer).

Results

Behavioral environment

For efficient experimentation, rodent behavioral training is typically parallelized such that multiple animals are trained at the same time. This necessitates 'compartmentalization', that is, the sensory isolation of the individual experiments. To this end we designed a sound attenuated chamber made of medium-density fiberboards (MDF) and high-end acoustic foams. We provide a design file for a 50-by-50-by-50 cm sound attenuated box constructed in SketchUp freely available 3D modeling computer program (Figure 4A-B; https://github.com/hangyabalazs/Rodent_behavior_setup/, sound_attenuated_box.skp). The interior of the box was covered with dense stainless steel mesh fabric to filter electrical fields for carrying out low noise electrophysiological measurements. (Figure 4C). We tested three different configurations for sound attenuation and compared the obtained attenuation levels at different tone frequencies. Sound pressure level was measures by a calibrated microphone placed inside the behavioral chamber while tones were played by speakers positioned outside the apparatus.

Sound attenuation was achieved by a combination of the dense engineered MDF wood, sound absorbing foams or an acoustic insulation board and pyramid acoustic foams. The enclosure was built of MDF boards since dense wood fiber is known to effectively reduce both airborne and impact sound. We used sound absorbing foams (Hanno Sealing and Insulation Systems) designed for machine and commercial vehicle industries. In these foams the sound absorbing element is a combination of an open-cell polyurethane foam and a 25 µm surface skin coated with black synthetic fiber (Protecto product line). These foams were optimized for airborne sound absorption by converting sound energy to heat as a consequence of friction in the polyurethane cell framework. In our experience, these foams are pliable, easy to cut, handle and mount on vertical surfaces aided by self-adhesive coating. Sound absorbing foams were compared to a 15 mm acoustic insulation board (PhoneStar) used for sound insulating floors, walls and ceilings in the construction industry. The acoustic insulation board consists of a fluted cardboard shell and compacted quartz sand filling. The oscillation of loose sand grains converts acoustic energy into kinetic energy. According to specifications, the acoustic insulation board reduces airborne sound by 36 dB and impact sound by 21 dB. However, the boards are relatively heavy (18 kg/m^2) and there is some sand leakage after cutting to size. We found that while sound absorbing foams and the acoustic insulation board provided comparable levels of sound attenuation (Figure 4G), the foam was easier to work with. Although only tested in the 1 to 20 kHz range, based on our measurements and the industrial specifications we extrapolate that similar sound attenuation levels might be achieved in higher frequency ranges relevant for rodent ultrasonic communication. In addition, we used a 70 mm open-cell pyramid foam borrowed from the music studio and stage equipment industry (Alfacoustic) that absorbs higher frequencies and efficiently reduces resonance and echoes.

We used a calibrated microphone to measure sound attenuation levels achieved by three particular setups: 1) MDF + sound insulation board + pyramid foam (Figure 4D); 2) MDF + 50 mm thick sound absorbing foam Hanno Protecto 20 (Figure 4E); 3) MDF + 20 mm thick sound absorbing foam Hanno Protecto 50 + pyramid foam (Figure 4F). We played 80-100 dB pure tones at different frequencies ranging from 100 Hz to 20 kHz (our software and hardware limit) inside the enclosure and measured the attenuated sound outside the chamber. From 2 kHz, which corresponds to the lower limit of rodent hearing range (Koay et al., 2002), all three setups reduced the detected volume to 35-45 dB , which did not differ from ambient noise levels (Figure 4G). Thus both the sound insulation board and the sound absorbing foams achieved sufficient sound attenuation (Koay

et al., 2002) while the absorbing foams had superior physical qualities (lower weight and no sand leakage). Bill of materials for the three configurations are available on https://github.com/hangyabalazs/Rodent_behavior_setup (headfixed_setup_BOM.docx).

Behavioral apparatuses for multiple behavioral paradigms can fit inside the sound attenuated enclosure, including both freely moving (e.g. two-alternative forced choice, 5-choice serial reaction time task (Busse et al., 2011; Kim et al., 2016; McGaughy et al., 2002; Yang and Zador, 2012; Yoshida and Katz, 2011) and head-fixed (e.g. auditory go/no-go, Pavlovian conditioning (Cohen et al., 2012; Eshel et al., 2015; Hangya et al., 2015; Pinto et al., 2013; Sanders and Kepecs, 2012)) behaviors.

Head-restrained behaviors are becoming increasingly popular due to highly reproducible behavior paradigms with low variability and ease of electrophysiology and imaging experiments. We provide here a complete modular head-fixed design for combined behavior, electrophysiology and optogenetic experiments in mice (Figure 5). The environment is assembled from a combination of Thorlabs and custom parts. A 3D-printed lick port housing an LED, an infrared photodiode and corresponding infrared photosensor (https://sanworks.io/shop/viewproduct?productID=1010) is mounted on a xyz stage (Thorlabs). The photosensor and photodiode enables temporally precise registration of beam breakings made by the animals tongue to provide an accurate readout of the animal's response to sensory cues and reinforcement (Figure 5A-C). For head-fixation, a custom pair of metal head bar holders are used. It is important that the mouse is positioned comfortably in the head-restraint and can properly reach the lick port within its natural range of tongue movements (Figure 5A). Indeed, in our experience, the most common mode of failure in training is the inadequate positioning of the licking spout. Since mice differ in size and position of their head restraint implants, two opportunities of adjustment are built in the head-fixed setup. First, the mouse sits on 3D-printed (https://github.com/hangyabalazs/Rodent_behavior_setup/, stage_rect.skp) or laser-cut rectangular, walled stage that is mounted on a lab jack (Fisher) that allows for adjustments in height. Second, the lick port is attached to an xyz stage allowing fine spatial positioning of the licking spout with respect to the animal's snout – a crucial step for achieving stable head-fixed performance. Water delivery for reward and facial air puff are controlled by fast solenoid valves (Lee Company). We use the open source Bpod behavioral control system (Sanworks, https://sanworks.io/shop/viewproduct?productID=1014) for real-time behavioral control and monitor the animals through infrared cameras (Point Grey) using Bonsai open source computer vision software (http://www.open-ephys.org/bonsai/, (Lopes et al., 2014)) that allows the tracking of eyeblinks, licking, whole body movements or pupil diameter (Figure 5B). Bill of materials for the head-fixed setup are available at https://github.com/hangyabalazs/Rodent_behavior_setup (headfixed_setup_BOM.docx). This setup is suitable for combining head-fixed mouse behaviors with single neuron recording and optogenetic stimulation (Figure 5C).

Delivering calibrated tones

In behavioral experiments it is often important to parametrically control stimulus intensity, for instance to manipulate task difficulty. We developed a sound calibration protocol to precisely control the sound pressure level (dB SPL) of auditory stimuli that allows both playing tones of controlled intensity and sound equalization

(https://github.com/hangyabalazs/Rodent_behavior_setup/tree/master/sound_calibration/, TeensyCalibration.m).

A precision microphone was connected to a preamplifier digital converter and placed between the head bar holders to model the position of the animal's head in the head-fixed setup (Figure 6A). Pure sinusoidal tones from 1 to 21 kHz frequency (with 0.25, 0.5 or 1 kHz resolution) with a pre-defined arbitrary amplitude were loaded onto the Teensy board via Bpod and played in sequence. Actual dB SPL levels of the played tones were measured with the calibrated microphone using the free version of the spectrum analyzer software TrueRTA and fed back to the calibration protocol software (Figure 6B). The experimenter then selected the target dB SPL and the amplitudes of the sine waves were updated according to Equation 1:

$$L_0 - L = 20 \log_{10} \frac{A_0}{A}$$

$$A_0 = A \cdot 10^{\frac{L_0 - L}{20}}$$

where L is observed and L_0 is the target sound pressure level (dB SPL), A is the actual sine wave amplitude and A_0 is the target amplitude corresponding to L_0.

Based on this calibrated set of sound intensities, any target intensity can later be software generated using Equation 1 (Figure 6C). It should be noted that this protocol does not handle sounds above 21 kHz, since common commercially available speakers cannot efficiently play sounds above the human hearing range. However, provided specific equipment for ultrasounds is available, the code can easily be adjusted to the experimenter's needs.

Besides pure tones, the calibration protocol also produced calibrated white noise. The procedure was similar to the pure tone calibration described above. White noise (*WN*) was generated with a pre-assigned amplitude (A=0.2) using Equation 2:

$$WN = randn(1{,}6 \cdot 44100) \cdot A$$

A_0 was calculated for five separate frequencies (1, 2, 5, 10 and 20 kHz) using Equation 1 and their average was used to assign the new amplitude for *WN*. We would like to note that generating equalized white noise by mixing calibrated frequency components would also be possible.

Temporally precise delivery of visual and auditory stimuli

In order to correlate action potential firing of neurons with external stimuli, it is important to accurately control the timing of stimulus presentation. We demonstrate a method to deliver simple visual and auditory stimuli to mice with millisecond order temporal precision (see Methods and Figure 3 for details on the procedure). We measured the exact latency and jitter of stimulus presentation. It is important to note that while the jitter directly increases the measurement noise for action potential timing (Figure 2), measured mean latencies can be compensated for post hoc.

LEDs were used for visual stimuli. These were controlled by the Bpod behavioral control system through an open source printed circuit board ('port interface board', https://sanworks.io/shop/viewproduct?productID=1008). Stimulus intensity can be directly modulated from Bpod on a 1 to 255 scale. To assess temporal precision of light delivery, we measured the time delay from the commanding TTL signal to the signal coming from the Bpod

port interface board LED pins (Figure 3B). Average light latency was 0.047 ± 0.003 ms (mean ± SD) (Figure 7B).

Temporally precise delivery of audio signals with short latency is a more complicated problem, since it requires a sound card that can store digital waveforms and send analog signals to speakers in order to play the sounds. Therefore, Bpod was connected to the microcontroller development system Teensy 3.2 and its audio adaptor board that was used as a serial slave device for playing sounds (Figure 6A-B). Pure tones were defined as sinewaves of characteristic frequencies in Matlab, with specific sampling rate, time duration and amplitude. The tones were uploaded to the Teensy system's SD memory card as a wav files using Bpod commands. Playing of the uploaded tracks were also triggered by Bpod. We measured the temporal delays from the TTL command onset to the onset of the analog signal sent from the Teensy adaptor board to the speakers (Figure 3D). Sound onset latency was 6.59 ± 0.9 ms (mean ± SD) (Figure 7C).

Temporally precise delivery of reinforcers

In associative learning paradigms, animals are rewarded and punished with appetitive and aversive stimuli, respectively. The temporally precise delivery of these stimuli, hereafter referred to as reinforcers, is paramount if we wish to understand how action potential firing of different neurons is related to these events. We equipped our setup with a system of solenoid valves and silicon tubing in order to deliver water reward and air puff punishment. We kept the distances short and attempted to avoid more bending then necessary to prevent longer delays in water or air delivery. We note however, that the exact latencies may depend on the tubing configuration, therefore we suggest performing delay measurements for every unique configurations (see details of tubing specifications in Materials and Methods). The opening and closing of valves that allow air and water flow was controlled by TTL pulses triggered by the Bpod system. To estimate the temporal precision of water and air delivery, we measured the time lags between the onset of the commanding TTL pulses and water or air leaving the tube system at the position of the animal's face.

We determined the time of water delivery by allowing the water droplet exiting the end of the delivery tubing to close an electric circuit by touching two wires positioned close to each other. Conversely, we measured air puff delivery by allowing the outflowing air wave to break a closed circuit by removing a drop of water from between two closely positioned wires. The rise (water) or fall (air) of the circuit signal was compared to a TTL pulse sent from Bpod concurrent with the valve command signals (Figure 3C). Latency of air delivery was 3.48 ± 0.02 ms (mean ± SD). Delay of water delivery was 8.61 ± 0.81 ms (mean ± SD) (Figure 7D-E).

Discussion

We presented a modular behavioral training environment to perform well-controlled, high-throughput behavioral assays in rodents. We provided a way of delivering audio-visual stimuli of calibrated intensity and measured the precise temporal latencies and jitters of stimulus and reinforcement delivery in this behavioral training solution. We believe this affordable modular system will allow streamlining behavioral experiments combined with electrophysiology and optogenetic manipulations.

Temporal control

Precise temporal control of the behaviorally relevant events of the task is essential for reliable estimation of spike timing with respect to those events. Major goals of a behavior control system that provides an ideal basis for electrophysiology were spelled out around the relatively recent birth of the rodent cognition field: "(1) interact rapidly with the experimental subjects […] the system should respond as fast as possible, and do so reliably; (2) provide high-time-resolution measurements of the events that have occurred, so as to get reliable time traces of behavior when combining it with electrophysiology; (3) be flexible yet easy to program and modify" (http://brodywiki.princeton.edu/bcontrol/). These principles lead to the design of BControl, a behavior control system relying on the precision of the Real Time Linux State Machine. This system fulfilled the first two goals really well, and the third one as well at then state-of-the-art. What has changed is the increasing availability of cheap and easy-to-program microcontrollers, which now allow almost the same level of precision but with a considerably less bulky system. Instead of the combination of a Windows machine, a complicated Real Time Linux machine, an expensive data acquisition card and correspondingly complex governing code, a single microcontroller with significantly simpler software interface can fulfill the goals delineated above (Sanders and Kepecs, 2012, 2014).

Some labs moved in the direction of automating behavioral training (Erlich et al., 2011) or even electrophysiological recordings from behaving animals (Dhawale et al., 2015). As these systems have clear benefits, we anticipate that they will be tremendously useful in the future. Nevertheless, they require considerably more resources than the simple system presented here. Also, we see the advantage of our system in its near-complete flexibility, which may be more useful during the planning, developing and troubleshooting phases of the experiments. In addition, our system also carries the possibility of multiplying into large scale, automated systems.

Spatial control

Head-fixed experimental paradigms has been criticized because the animals are artificially restricted in their natural movements. While true, this also has an often overlooked flip side. Constraining the space of possible behavioral patterns of the animal means better behavioral control at the same time, as it decreases the uncontrolled behavioral variability and hence the uncontrolled variability ('noise') of the electrophysiological recordings. In addition, it allows optical imaging of neural activity under fixed microscopes – an often exploited advantage (Chen et al., 2013). Thus these experiments are highly repeatable and offer a good opportunity to investigate neuronal mechanisms in non-anesthetized, behaving animals in a large number of repeated trials within one session (Guo et al., 2014; Micallef et al., 2017). Accordingly, head-fixed experimental procedures are becoming increasingly popular in studying neural mechanisms of sensation, cognition and other behaviors in rodents (Abraham et al., 2012; Dolzani et al., 2014; O'Connor et al., 2010; Peters et al., 2014; Saleem et al., 2017; Yu et al., 2016).

Nevertheless, many of the behavioral paradigms require free motion of the animals. For instance, although there are an increasing number of very useful virtual reality systems for rodents (Harvey et al., 2009; Keller et al., 2012), many of the spatial learning paradigms are still performed in freely behaving animals. In addition, an important line of research is addressing the more naturalistic animal behaviors including, but not restricted to motor learning and execution, in which case minimizing the artificial constraints is inherent to the experiment (Kawai et al., 2015; Lopes et al.,

2017). How do we achieve the best possible spatial control in these experiments? We argue that tracking the spatial position of the animal or its specific parts (limbs, joints, head, tail, etc.) to the same level of precision as compared with other aspects of their behavior is crucial. Not only does it allow precise registering of action potential firing with respect to spatial cues, it also opens the possibility of closed-loop stimulation based on position. Note that the open source Bonsai software operating on the principle of parallel asynchronous streams is well suited for these tasks (Lopes et al., 2014).

Concluding remark

We demonstrated a modular, flexible, affordable, largely open source solution for rodent behavior with sufficient temporal precision for electrophysiology and optogenetic experiments. We anticipate a continuing growth of the technical armaments of behavioral neurophysiology suited for ever-increasing temporal and spatial control. Sharing new tools within the scientific community is important in order to facilitate this technical development. Design files, Matlab code, bill of materials and other documents pertaining to the present report can be downloaded from https://github.com/hangyabalazs/Rodent_behavior_setup/.

Figures

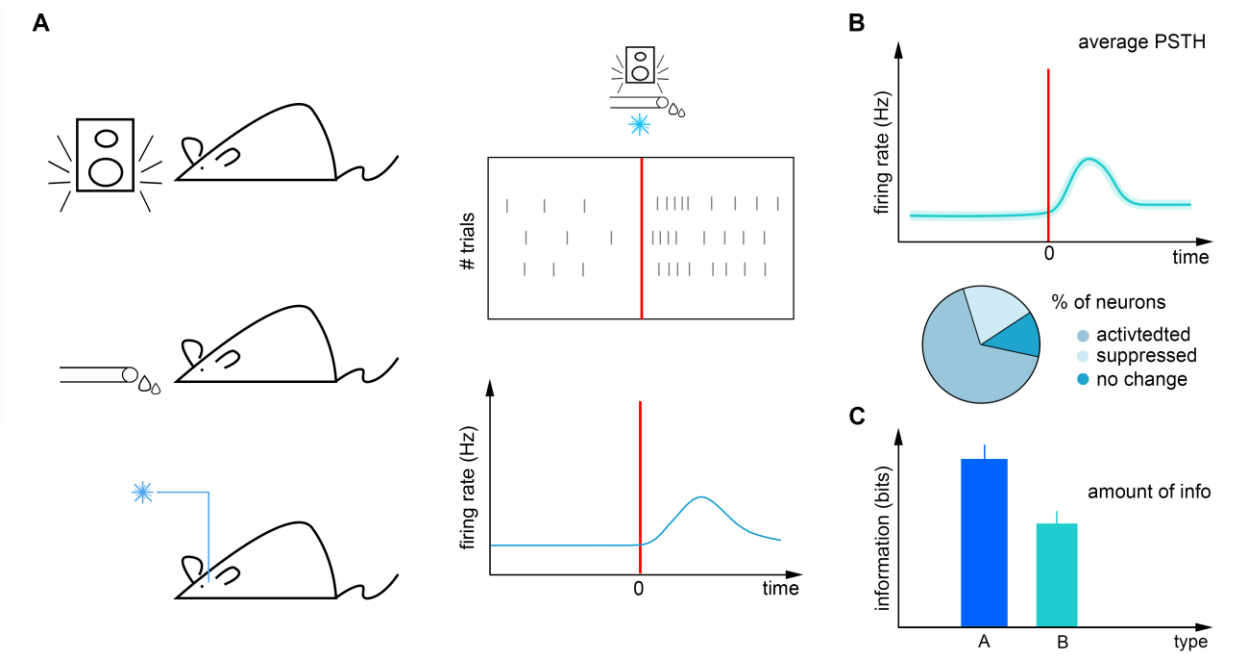

Figure 1. **Firing rate analysis. (A)** Left, mice are exposed to temporally controlled sensory cues, reinforcers and external neural stimulation. Right, neural activity (black ticks) can be aligned to these events in raster plots (top) and peri-event time histograms (bottom). **(B)** Neurons can be categorized according to their tuning to these events. **(C)** The information carried by neural responses about external events can be quantified by information theory tools.

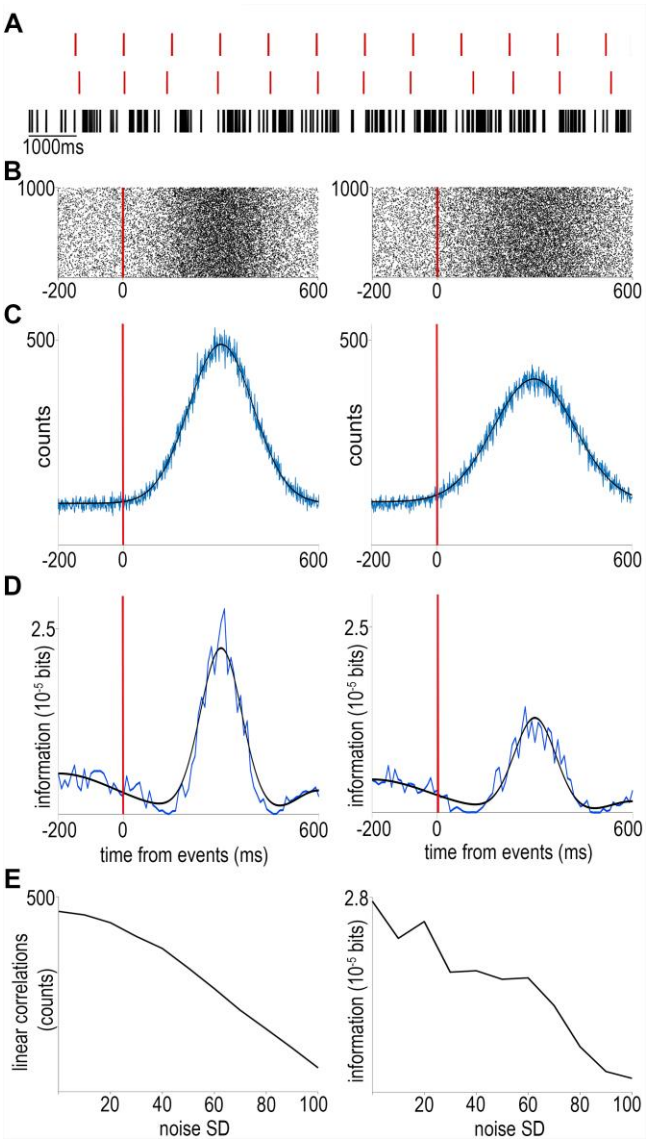

Figure 2. The effects of noise on event timing. (A) We simulated an event train without (top) or with Gaussian noise (middle) as well as a spike train consisting of 'stimulus-evoked' spikes according to a normal distribution and background Poisson spiking (bottom). **(B)** Raster plots aligned to noiseless (left) or noisy (right) events. **(C)** Peri-event time histograms (equivalent to event-spike cross-correlations) corresponding to the raster plots above. Blue, raw traces; black, Gaussian fits. **(D)** Mutual information between spike times and event times without (left) or with (right) noise. Note the second increase of mutual information around 500 ms corresponding to the information on the event times carried by the lack of event-aligned spikes, demonstrating the power of information theory to detect non-linear correlations. **(E)** Both linear cross-correlation (left) and non-linear mutual information (right) decreases with the amount of added noise in event timing. Code is available at https://github.com/hangyabalazs/Rodent_behavior_setup/, Experiment_simulation.m.

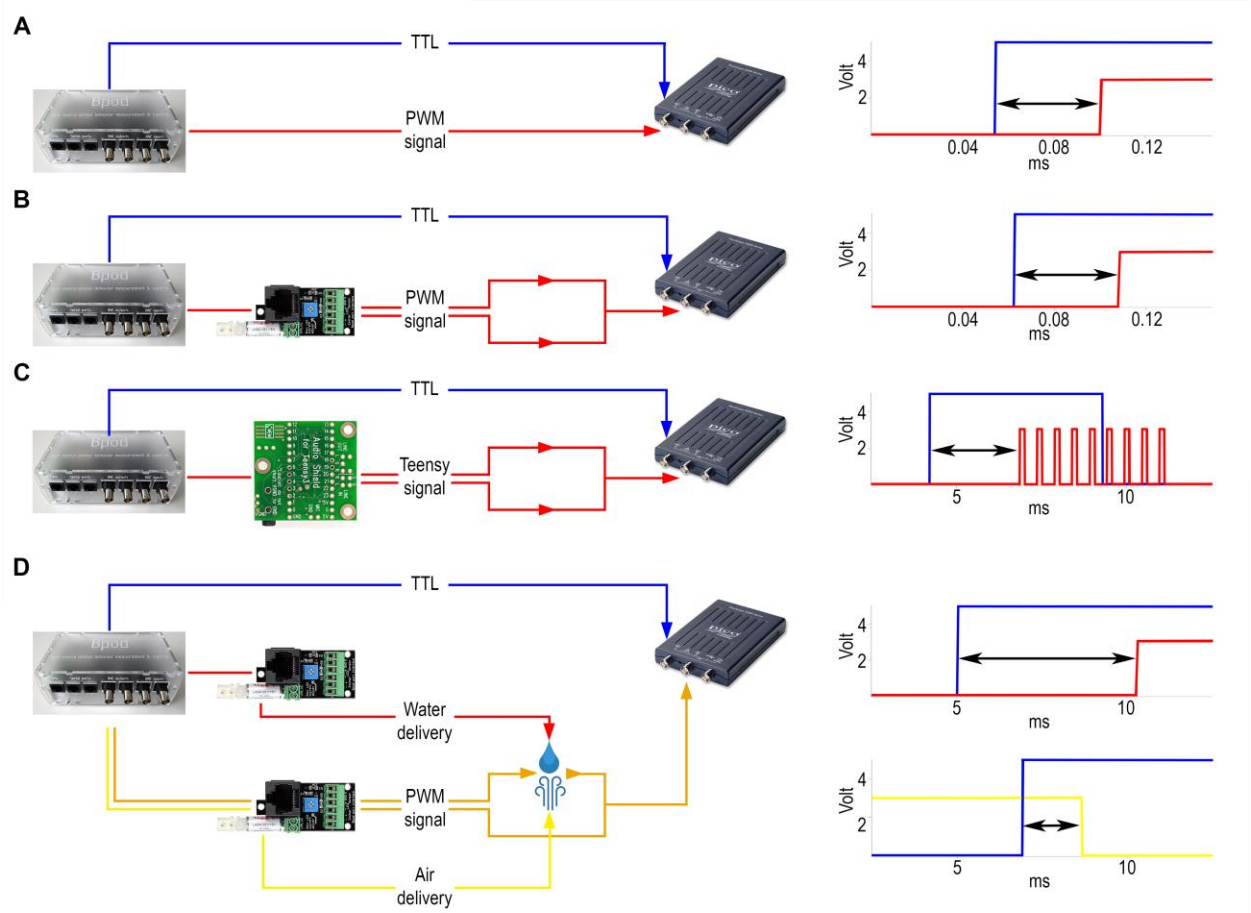

Figure 3. Delay measurements. (A) Internal delay. Left, signals were sent from the BNC output port (blue) and the RJ45 output connector for communication with the port interface board (red) directly to the oscilloscope. Right, example signals detected by the oscilloscope. Arrow, measured delay **(B)** Delay of visual cue. Left, signals were sent from Bpod to the oscilloscope both directly (blue) and via the port interface board (red). Right, example of the signals detected by the oscilloscope. **(C)** Delay of sound delivery. Left, signals were sent directly (blue) or via the Teensy board (red). The oscilloscope receives the latter signal from the line out pins of the Teensy slave board. Right, example of the signals detected by the oscilloscope. **(D)** Delay of reinforcement delivery. Left, signals were sent from the BNC output port (blue) directly to the oscilloscope and to two port interface boards. One port was receiving commands to open and close the water valve (red), while the other was receiving similar input for controlling the air valve (yellow) along with a constant PWM signal (orange). The latter was sent to the oscilloscope throughout a circuit that water or air could close or break, respectively, changing the oscilloscope voltage input. Top right, example of the signals detected by the oscilloscope for water delay measurement. Bottom right, example of the signals detected by the oscilloscope for air delay measurement.

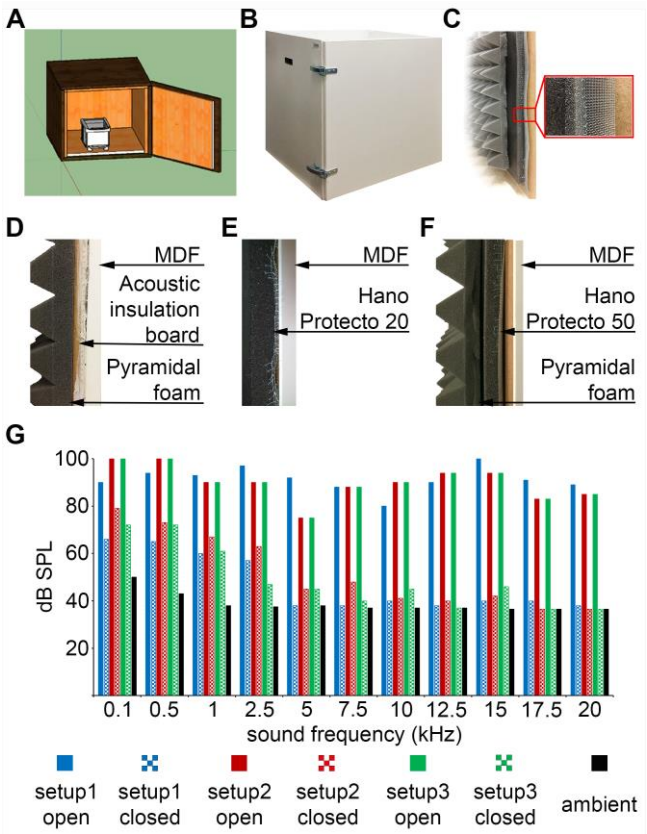

Figure 4. Custom-made sound-attenuated enclosures. **(A)** Blueprint and **(B)** physical implementation of the box designed to host the behavioral-recording setup. **(C)** Cross-section of the box: from left to right, pyramidal foam, sound absorbing foam, stainless steel mesh and medium-density fiberboard (MDF). **(D)** Configuration #1: sound attenuation by acoustic insulation board with quartz sand filling and pyramidal foam. **(E)** Configuration #2: Hanno Protecto 20 foam. **(F)** Configuration #3: Hanno Protecto 50 foam combined with pyramidal foam. **(G)** Sound attenuation measurements: pure tones of different pitch were played from speakers outside the enclosure and the dB SPL was measured by a microphone placed inside with the door open or closed.

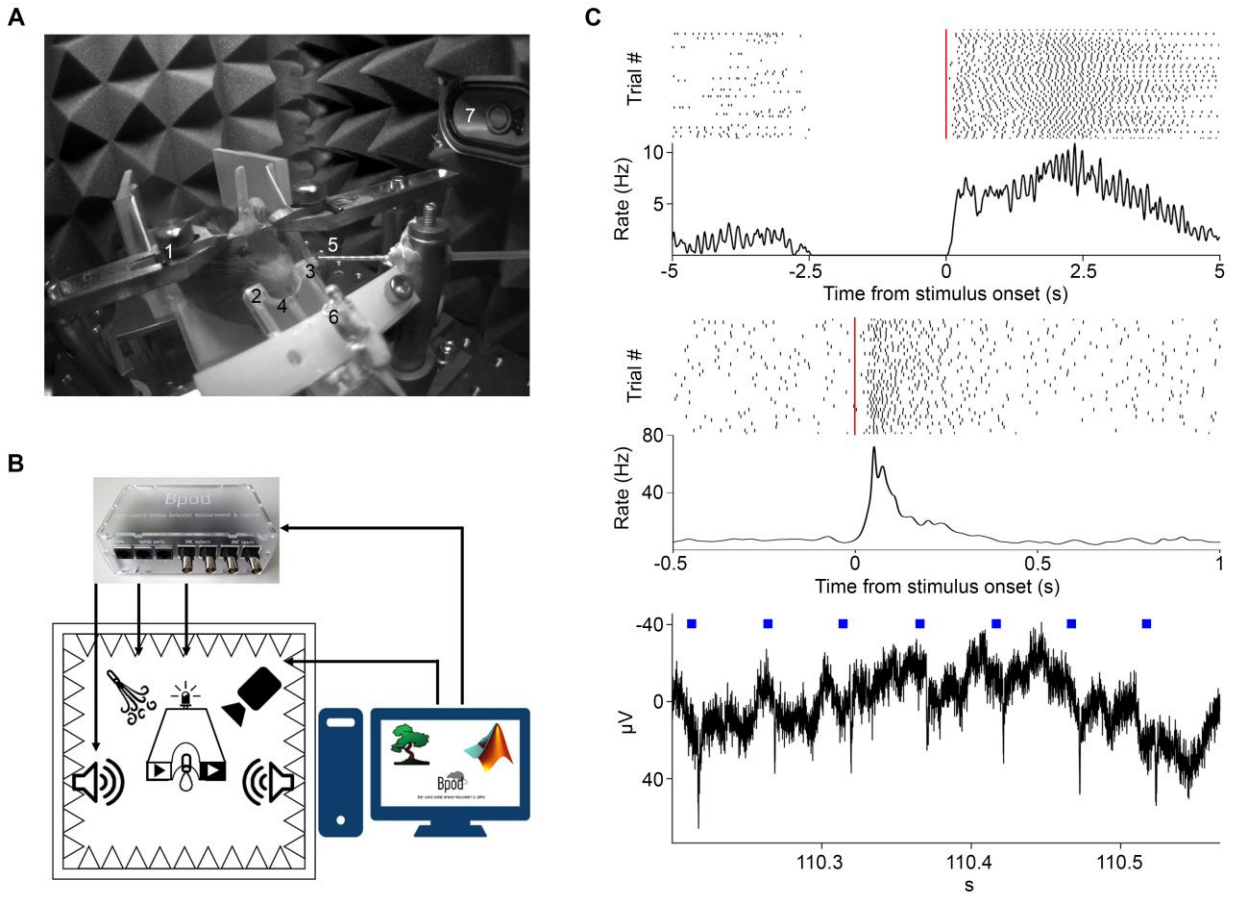

Figure 5. Head-fixed setup. (A) The animal is held by an implanted head bar with a pair of metal holders (1), facing a custom-made lick port hosting an IR emitter and an IR receiver (2, 3) for lick detection and a plastic water spout (4). Air-puff is delivered via a cannula placed near the animal's face (5). Visual and auditory cues are delivered by a central LED (6) and lateral speakers (7). **(B)** Schematic diagram of the behavior setup. Cue and reinforcement delivery are controlled by Bpod. Motion is monitored with a camera using Bonsai open software. (C) Top, raster plot of lick responses (black ticks) to reward-predicting cues (red line) of a mouse trained on an auditory Pavlovian task. Middle, raster plot of action potentials (black ticks) of a neuron responding to the reward-predicting cue (red line) in the same task. Bottom, local filed potential deflections in response to photostimulation (blue squares) in a mouse expressing the light-sensitive channelrhodopsin.

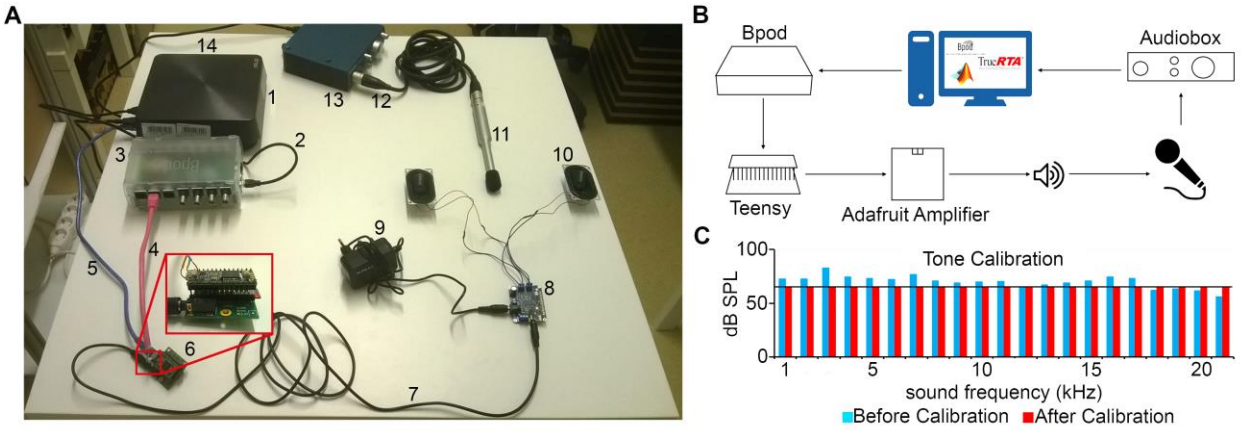

Figure 6. Sound calibration and delivery. (A) Components: computer (1), miniUSB-USB A cable (2), Bpod (3), ethernet cable (4), miniUSB-USB A cable (5), Audio Adaptor Board for Teensy + Teensy USB Development Board + SD card (6), 3.5mm stereo jack to jack cable (7), Adafruit Audio Amplifier (8), 12V power supply (9), Digikey 8 Ohm Magnetic Speakers (10), EMM-6 Electret Measurement Microphone (11), Male-Female three-pin XLR cable (12), AudioBox iOne (13), USB B -USB A cable (14). **(B)** Schematic of the setup. A sine wave is generated in Matlab and sent to Bpod, which loads it to the Teensy apparatus as a .wav file. When played by the speakers, the sound is detected by the microphone, delivered to the computer and the dB SPL is read by the TrueRTA software. **(C)** The dB SPL levels at each frequency before (blue) and after (red) the calibration process. Solid black line indicates the calibration target volume (60 dB SPL).

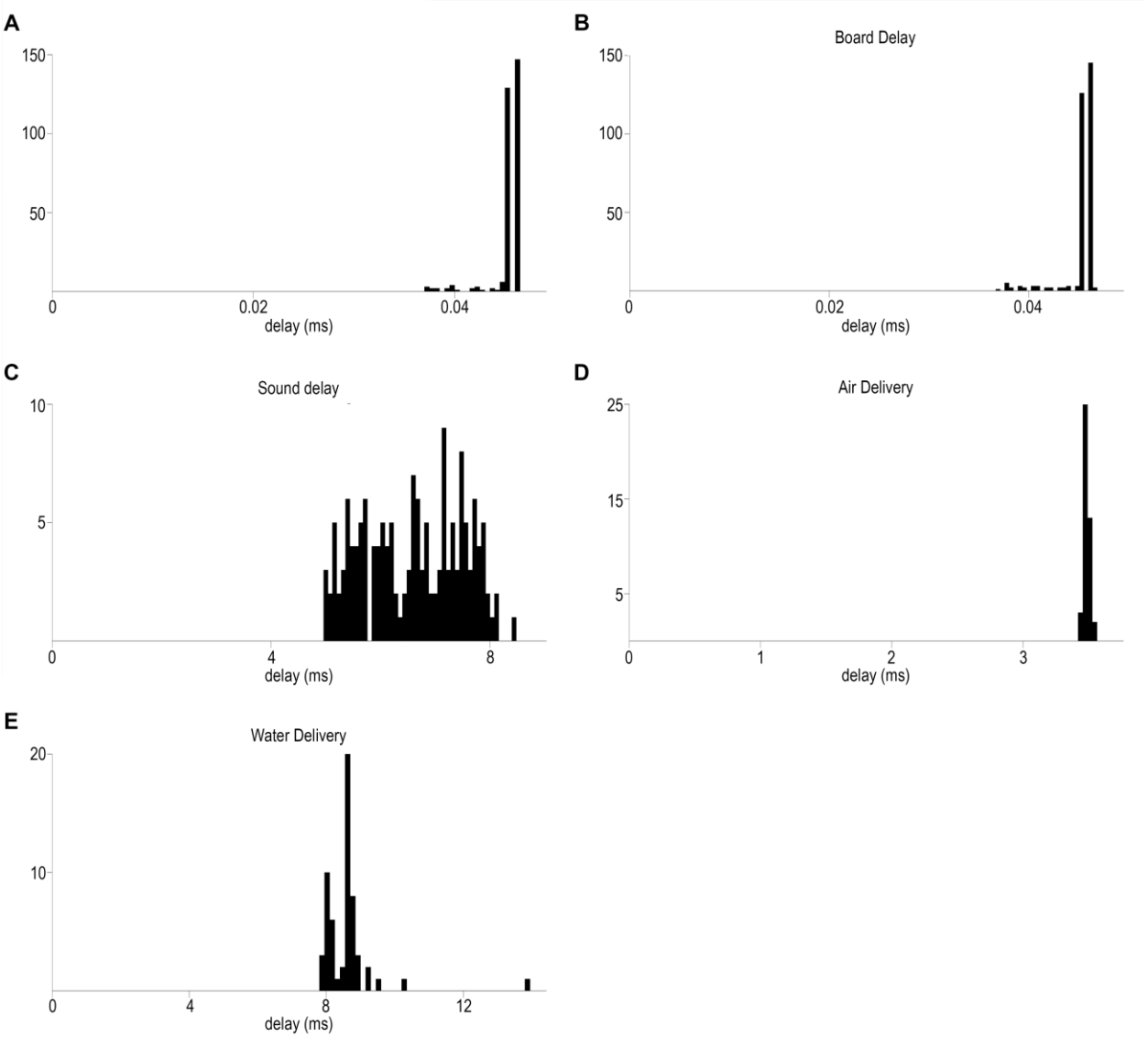

Figure 7. Temporally precise delivery of stimuli and feedback. (A) Distribution of minimal elapsed time between sending signals to the BNC and RJ45 output of Bpod (mean ± SD, 0.045 ± 0.001 ms). **(B)** Board delay: distribution of delays between the signals from the BNC output port and the LED output wire terminal of the port interface board (mean ± SD, 0.047 ± 0.003 ms) **(C)** Delay distribution of sound delivery, between the signals from the BNC output port and the Teensy board (mean ± SD, 6.59ms ± 0.9 ms). **(D)** Delay distribution of air puff delivery (mean ± SD, 3.48 ± 0.02 ms). **(E)** Delay distribution of water delivery (mean ± SD, 8.61 ± 0.81 ms).

Ethics Statement

All experiments were approved by the Committee for the Scientific Ethics of Animal Research of the National Food Chain Safety Office (PE/EA/675-4/2016) and were performed according to the guidelines of the institutional ethical code and the Hungarian Act of Animal Care and Experimentation (1998; XXVIII, section 243/1998, renewed in 40/2013) in accordance with the European Directive 86/609/CEE and modified according to the Directives 2010/63/EU.

Author Contributions

BH developed the idea and conceptualized the manuscript. KS and PH designed the behavioral environment. PH performed combined experiments of behavior, electrophysiology and optogenetics. NS, TL and AS performed the delay measurements. NS developed the sound delivery system and performed all sound measurements. NS and BH performed the simulations. NS and KS generated the figures. BH and NS wrote the manuscript with input from all authors.

Acknowledgement

We thank Ranade P. Sachin and Rob Eifert for parts of the head-fixing apparatus, Péter Barthó and Sándor Borbély for their input on the sound attenuated enclosure, Joshua I. Sanders and András Széll for help with the Bpod system and the delay measurements, Adam Kepecs for concepts and discussions. This work was supported by the 'Lendület' Program of the Hungarian Academy of Sciences (LP2015-2/2015) and the European Research Council Starting Grant no. 715043. BH is a member of the FENS-Kavli Network of Excellence.

References

Abraham, N. M., Guerin, D., Bhaukaurally, K., and Carleton, A. (2012). Similar Odor Discrimination Behavior in Head-Restrained and Freely Moving Mice. *PLoS One* 7. doi:10.1371/journal.pone.0051789.

Arabzadeh, E., Panzeri, S., and Diamond, M. E. (2006). Deciphering the Spike Train of a Sensory Neuron : Counts and Temporal Patterns in the Rat Whisker Pathway. 26, 9216–9226. doi:10.1523/JNEUROSCI.1491-06.2006.

Brunton, B. W., Botvinick, M. M., and Brody, C. D. (2013). Rats and humans can optimally accumulate evidence for decision-making. *Science (80-.).* 340, 95–8. doi:10.1126/science.1233912.

Busse, L., Ayaz, A., Dhruv, N. T., Katzner, S., Saleem, A. B., Schölvinck, M. L., et al. (2011). The Detection of Visual Contrast in the Behaving Mouse. *J. Neurosci.* 31, 11351–11361. doi:10.1523/jneurosci.6689-10.2011.

Chen, J. L., Andermann, M. L., Keck, T., Xu, N.-L., and Ziv, Y. (2013). Imaging Neuronal Populations in Behaving Rodents: Paradigms for Studying Neural Circuits Underlying Behavior in the Mammalian Cortex. *J. Neurosci.* 33, 17631–17640. doi:10.1523/JNEUROSCI.3255-13.2013.

Cohen, J. Y., Haesler, S., Vong, L., Lowell, B. B., and Uchida, N. (2012). Neuron-type-specific signals for reward and punishment in the ventral tegmental area. *Nature* 482, 85–8. doi:10.1038/nature10754.

Csiszár, I., and Körner, J. (2011). *Information theory : coding theorems for discrete memoryless systems*. Cambridge University Press.

Dhawale, A. K., Poddar, R., Kopelowitz, E., Normand, V., Wolff, S., and Olveczky, B. (2015).

Automated long-term recording and analysis of neural activity in behaving animals. *bioRxiv* 33266, 33266. doi:10.1101/033266.

Diamond, M. E., von Heimendahl, M., Knutsen, P. M., Kleinfeld, D., and Ahissar, E. (2008). "Where" and "what" in the whisker sensorimotor system. *Nat Rev Neurosci* 9, 601–612. doi:10.1038/nrn2411.

Dolzani, S. D., Nakamura, S., and Cooper, D. C. (2014). A novel variable delay Go/No-Go task to study attention, motivation and working memory in the head-fixed rodent. *F1000Research*. doi:10.12688/f1000research.2-125.v2.

Endres, D., Oram, M., Schindelin, J., and Foldiak, P. (2008). Bayesian binning beats approximate alternatives: estimating peri-stimulus time histograms. *Adv. Neural Inf. Process. Syst. 2007*, 393–400.

Erlich, J. C., Bialek, M., and Brody, C. D. (2011). A cortical substrate for memory-guided orienting in the rat. *Neuron* 72, 330–343. doi:10.1016/j.neuron.2011.07.010.

Eshel, N., Bukwich, M., Rao, V., Hemmelder, V., Tian, J., and Uchida, N. (2015). Arithmetic and local circuitry underlying dopamine prediction errors. *Nature* 525, 243–246. doi:10.1038/nature14855.

Guo, Z. V., Hires, S. A., Li, N., O'Connor, D. H., Komiyama, T., Ophir, E., et al. (2014). Procedures for behavioral experiments in head-fixed mice. *PLoS One* 9. doi:10.1371/journal.pone.0088678.

Hangya, B., Ranade, S. P., Lorenc, M., and Kepecs, A. (2015). Central Cholinergic Neurons Are Rapidly Recruited by Reinforcement Feedback. *Cell* 162, 1155–1168. doi:10.1016/j.cell.2015.07.057.

Hanks, T. D., Kopec, C. D., Brunton, B. W., Duan, C. A., Erlich, J. C., and Brody, C. D. (2015). Distinct relationships of parietal and prefrontal cortices to evidence accumulation. *Nature* 520, 220–3. doi:10.1038/nature14066.

Harvey, C. D., Collman, F., Dombeck, D. A., and Tank, D. W. (2009). Intracellular dynamics of hippocampal place cells during virtual navigation. *Nature* 461, 941–946. doi:10.1038/nature08499.

Jaramillo, S., and Zador, A. M. (2011). The auditory cortex mediates the perceptual effects of acoustic temporal expectation. *Nat Neurosci* 14, 246–251. doi:http://www.nature.com/neuro/journal/v14/n2/abs/nn.2688.html#supplementary-information.

Kawai, R., Markman, T., Poddar, R., Ko, R., Fantana, A. L., Dhawale, A. K., et al. (2015). Motor Cortex Is Required for Learning but Not for Executing a Motor Skill. *Neuron* 86, 800–812. doi:10.1016/j.neuron.2015.03.024.

Kayser, C., Logothetis, N. K., and Panzeri, S. (2010). Millisecond encoding precision of auditory cortex neurons. 107. doi:10.1073/pnas.1012656107.

Keller, G. B., Bonhoeffer, T., and Hübener, M. (2012). Sensorimotor Mismatch Signals in Primary Visual Cortex of the Behaving Mouse. *Neuron* 74, 809–815.

doi:10.1016/j.neuron.2012.03.040.

Kim, H., Ährlund-Richter, S., Wang, X., Deisseroth, K., and Carlén, M. (2016). Prefrontal Parvalbumin Neurons in Control of Attention. *Cell* 164, 208–218. doi:10.1016/j.cell.2015.11.038.

Koay, G., Heffner, R. S., and Heffner, H. E. (2002). Behavioral audiograms of homozygous medJ mutant mice with sodium channel deficiency and unaffected controls. *Hear. Res.* 171, 111–118. doi:10.1016/S0378-5955(02)00492-6.

Kvitsiani, D., Ranade, S., Hangya, B., Taniguchi, H., Huang, J. Z., and Kepecs, A. (2013). Distinct behavioural and network correlates of two interneuron types in prefrontal cortex. *Nature* 498, 363–6. doi:10.1038/nature12176.

Lima, S. Q., Hromádka, T., Znamenskiy, P., and Zador, A. M. (2009). PINP: a new method of tagging neuronal populations for identification during in vivo electrophysiological recording. *PLoS One* 4, e6099. doi:10.1371/journal.pone.0006099.

Lin, S.-C., and Nicolelis, M. a L. (2008). Neuronal ensemble bursting in the basal forebrain encodes salience irrespective of valence. *Neuron* 59, 138–49. doi:10.1016/j.neuron.2008.04.031.

Lopes, G., Bonacchi, N., Frazão, J., and Neto, J. (2014). Bonsai: An event-based framework for processing and controlling data streams. *bioRxiv*. doi:10.1101/006791.

Lopes, G., Nogueira, J., Dimitriadis, G., Menendez, J. A., Paton, J. J., and Kampff, A. R. (2017). A robust role for motor cortex. *bioRxiv*. Available at: http://www.biorxiv.org/content/early/2017/05/18/058917 [Accessed September 13, 2017].

McGaughy, J., Dalley, J. W., Morrison, C. H., Everitt, B. J., and Robbins, T. W. (2002). Selective behavioral and neurochemical effects of cholinergic lesions produced by intrabasalis infusions of 192 IgG-saporin on attentional performance in a five-choice serial reaction time task. *J. Neurosci.* 22, 1905–13.

Micallef, A. H., Takahashi, N., Larkum, M. E., and Palmer, L. M. (2017). A Reward-Based Behavioral Platform to Measure Neural Activity during Head-Fixed Behavior. *Front. Cell. Neurosci.* 11. doi:10.3389/fncel.2017.00156.

O'Connor, D. H., Clack, N. G., Huber, D., Komiyama, T., Myers, E. W., and Svoboda, K. (2010). Vibrissa-Based Object Localization in Head-Fixed Mice. *J. Neurosci.* 30, 1947–1967. doi:10.1523/JNEUROSCI.3762-09.2010.

Panzeri, S., Harvey, C. D., Piasini, E., Latham, P. E., and Fellin, T. (2017). Cracking the Neural Code for Sensory Perception by Combining Statistics, Intervention, and Behavior. *Neuron* 93, 491–507. doi:10.1016/j.neuron.2016.12.036.

Peters, A. J., Chen, S. X., and Komiyama, T. (2014). Emergence of reproducible spatiotemporal activity during motor learning. *Nature* 510, 263–267. doi:10.1038/nature13235.

Pi, H.-J., Hangya, B., Kvitsiani, D., Sanders, J. I., Huang, Z. J., and Kepecs, A. (2013). Cortical interneurons that specialize in disinhibitory control. *Nature* 503, 521–524.

Pinto, L., Goard, M. J., Estandian, D., Xu, M., Kwan, A. C., Lee, S.-H., et al. (2013). Fast modulation of visual perception by basal forebrain cholinergic neurons. *Nat. Neurosci.* 16, 1857–63. doi:10.1038/nn.3552.

Poddar, R., Kawai, R., Ölveczky, B. P., Matsumoto, K., and Squire, L. (2013). A Fully Automated High-Throughput Training System for Rodents. *PLoS One* 8, e83171. doi:10.1371/journal.pone.0083171.

Ranade, S. P., and Mainen, Z. F. (2009). Transient firing of dorsal raphe neurons encodes diverse and specific sensory, motor, and reward events. *J. Neurophysiol.* 102, 3026–37. doi:10.1152/jn.00507.2009.

Raposo, D., Sheppard, J. P., Schrater, P. R., and Churchland, A. K. (2012). Multisensory decision-making in rats and humans. *J. Neurosci.* 32, 3726–3735. doi:10.1523/JNEUROSCI.4998-11.2012.

Saleem, A. B., Lien, A. D., Krumin, M., Haider, B., Rosón, M. R., Ayaz, A., et al. (2017). Subcortical Source and Modulation of the Narrowband Gamma Oscillation in Mouse Visual Cortex. *Neuron* 93, 315–322. doi:10.1016/j.neuron.2016.12.028.

Sanders, J. I., and Kepecs, A. (2012). Choice ball: a response interface for two-choice psychometric discrimination in head-fixed mice. *J. Neurophysiol.* 108, 3416–3423. doi:10.1152/jn.00669.2012.

Sanders, J. I., and Kepecs, A. (2014). A low-cost programmable pulse generator for physiology and behavior. *Front. Neuroeng.* 7. doi:10.3389/fneng.2014.00043.

Shimazaki, H., and Shinomoto, S. (2010). Kernel bandwidth optimization in spike rate estimation. *J. Comput. Neurosci.* 29, 171–182. doi:10.1007/s10827-009-0180-4.

Tiesinga, P., Fellous, J.-M., and Sejnowski, T. J. (2008). Regulation of spike timing in visual cortical circuits. *Nat. Rev. Neurosci.* 9, 97–107. doi:10.1038/nrn2315.

Yang, Y., and Zador, A. M. (2012). Differences in Sensitivity to Neural Timing among Cortical Areas. *J. Neurosci.* 32, 15142–15147. doi:10.1523/JNEUROSCI.1411-12.2012.

Yoshida, T., and Katz, D. B. (2011). Control of Prestimulus Activity Related to Improved Sensory Coding within a Discrimination Task. *J. Neurosci.* 31, 4101–4112. doi:10.1523/jneurosci.4380-10.2011.

Yu, K., Garcia da Silva, P., Albeanu, D. F., and Li, B. (2016). Central Amygdala Somatostatin Neurons Gate Passive and Active Defensive Behaviors. *J. Neurosci.* 36, 6488–6496. doi:10.1523/JNEUROSCI.4419-15.2016.

Zuo, Y., Safaai, H., Notaro, G., Mazzoni, A., Panzeri, S., and Diamond, M. E. (2015). Complementary Contributions of Spike Timing and Spike Rate to Perceptual Decisions in Rat S1 and S2 Cortex. *Curr. Biol.* 25, 357–363. doi:10.1016/j.cub.2014.11.065.